NIH Public Access
Author Manuscript
Invest Ophthalmol Vis Sci. Author manuscript; available in PMC 2010 October 5.

Published in final edited form as:
Invest Ophthalmol Vis Sci. 2002 April ; 43(4): 1176–1181.

Functional Magnetic Resonance Imaging of the Retina

Timothy Q. Duong[1], **Shing-Chung Ngan**[2], **Kamil Ugurbil**[3], and **Seong-Gi Kim**[3]

[1] Center for Comparative NeuroImaging, Department of Psychiatry, University of Massachusetts Medical School, Worcester, Massachusetts

[2] Department of Microbiology, University of Washington, Seattle, Washington

[3] Center for Magnetic Resonance Research, Department of Radiology, University of Minnesota Medical School, Minneapolis, Minnesota

Abstract

Purpose—This study explored the feasibility of mapping the retina's responses to visual stimuli noninvasively, by using functional magnetic resonance imaging (fMRI).

Methods—fMRI was performed on a 9.4-Tesla scanner to map activity-evoked signal changes of the retina–choroid complex associated with visual stimulation in anesthetized cats ($n = 6$). Three to 12 1-mm slices were acquired in a single shot using inversion-recovery, echo-planar imaging with a nominal in-plane resolution of $468 \times 468\ \mu m^2$. Visual stimuli were presented to the full visual field and to the upper and lower visual fields. The stimuli were drifting or stationary gratings, which were compared with the dark condition. Activation maps were computed using cross-correlation analysis and overlaid on anatomic images. Multislice activation maps were reconstructed and flattened onto a two-dimensional surface.

Results—fMRI activation maps showed robust increased activity in the retina–choroid complex after visual stimulation. The average stimulus-evoked fMRI signal increase associated with drifting-grating stimulus was 1.7% ± 0.5% ($P < 10^{-4}$, $n = 6$) compared with dark. Multislice functional images of the retina flattened onto a two-dimensional surface showed relatively uniform activation. No statistically significant activation was observed in and around the optic nerve head. Hemifield stimulation studies demonstrated that stimuli presented to the upper half of the visual field activated the lower part of the retina, and stimuli presented to the lower half of the visual field activated the upper part of the retina, as expected. Signal changes evoked by the stationary gratings compared with the dark basal condition were positive but were approximately half that evoked by the drifting gratings (1.0% ± 0.1% versus 2.1% ± 0.3%, $P < 10^{-4}$).

Conclusions—To the best of our knowledge, this is the first fMRI study of the retina, demonstrating its feasibility in imaging retinal function dynamically in a noninvasive manner and at relatively high spatial resolution.

The retina is more than an array of light sensors. It is a part of the central nervous system, and it generally performs complex signal processing before sending its signals to the lateral geniculate nucleus and the visual cortex.[1] Metabolism and blood flow of the retina are complex and in many aspects unique.[2] For example, being only approximately 250 μm thick, the retina is one of the most vascularized tissues in the body, has one of the highest oxidative metabolic rates per tissue weight,[3] and yet still manages to produce an inordinate amount of lactate under basal conditions. The retina is nourished by the retinal and choroidal blood supplies,[4] which

Corresponding author: Timothy Q. Duong, Department of Psychiatry, University of Massachusetts Medical School, Worcester, MA 01655; timothy.duong@umassmed.edu.

Commercial relationships policy: N.

NIH-PA Author Manuscript
NIH-PA Author Manuscript
NIH-PA Author Manuscript

NIH-PA Author Manuscript

NIH-PA Author Manuscript

NIH-PA Author Manuscript

feed the inner and the outer retina, respectively. Oxygen transport into the highly structured layers of cells in the retina relies heavily on diffusion, with oxygen tension midway between the inner and outer retina approaching close to hypoxic levels under normal physiological conditions.[5] Hence, the retina is particularly susceptible to ischemic injuries, as in the case of diabetic retinopathy.[6,7] The choroidal blood flow, which feeds the outer retina including the photoreceptors, is many times higher than the cortical blood flow.[8–10] It has been suggested that such high blood flow is necessary for maintaining retinal oxygenation[11] and for dissipating heat produced by the incident light on the retina,[12,13] although these issues remain controversial.

Retinal physiology and function have been studied by using a number of methods, including, but not limited to, standard psychophysical evaluation, standard[14] and multifocal[15] electroretinography, oxygen microelectrodes,[5] laser Doppler flowmetry,[16,17] blue-field entoptic technique,[18] and fluorescein angiography.[19] These techniques can provide valuable functional and physiological information on the retina in research and/or clinical settings. Most of these techniques require an unobstructed pathway of light from the cornea through the lens and to the retina. Disease states with media opacity, such as cataract and some diseases of the vitreous body, preclude the use of many of these techniques. Vitreous humor oxygen tension has been assessed by measuring water relaxation time.[20] This technique, however, has poor sensitivity and is only useful for measuring large and steady-state oxygenation changes in the vitreous humor. Therefore, noninvasive and dynamic imaging of the retina and its functional response to visual stimuli at the tissue level, without depth limitation and in three dimensions by using functional magnetic resonance imaging (fMRI), could have numerous important applications. This method is also expected to complement other techniques mentioned.

fMRI is a powerful, noninvasive imaging method capable of high spatial resolution. It has been widely used in imaging brain processes, ranging from sensory perceptions to cognitive functions. The most commonly used fMRI technique is based on blood oxygenation level–dependent (BOLD) contrast, first described by Ogawa et al.[21] in rat brains and subsequently used for mapping brain functions in humans.[22–24] BOLD contrast originates from the intravoxel magnetic field's inhomogeneticity, which is induced by paramagnetic deoxyhemoglobin in the erythrocytes in blood. Magnetic susceptibility differences between the compartmentalized paramagnetic deoxyhemoglobin in blood and the surrounding tissues generate magnetic field gradients across and near the vascular–tissue boundary. Changes in regional deoxyhemoglobin content can be visualized in susceptibility-sensitized (T_2*- or T_2-weighted) BOLD images. When a specific task (e.g., finger tapping) is performed, regional cerebral blood flow increases disproportionally, overcompensating the stimulus-induced oxygen-consumption rate increase needed to fuel the increased neural activity and thus resulting in a regional reduction in deoxyhemoglobin concentration. Therefore, BOLD signals after elevated neural activity increase compared with basal conditions, making it possible to dynamically and noninvasively map changes in neural activities.

There is considerable evidence that visual stimuli evoke changes in tissue blood flow and tissue oxygen tension in the retina. Riva et al.[25] and Longo et al.[26] demonstrated with laser Doppler that blood flow in the retina increases after visual stimulation, and Scheiner et al.[27] reported stimulus-evoked changes in blood flow using a blue-field simulation technique. Linsenmeier et al.,[5] using oxygen electrode recording, showed that oxygenation in different retinal cell layers also increases after visual stimulation. Therefore, it is not unreasonable to postulate that a BOLD fMRI signal response could be detected, because the BOLD signal derives from changes in tissue oxygenation as a result of blood flow modulation. In this study, we explored the feasibility of extending functional MRI to image the retina's response to various visual stimuli. The difficulties and challenges of retinal fMRI are discussed, and the solutions to these problems are detailed. The results presented herein demonstrate that fMRI of the retina is a

NIH-PA Author Manuscript

NIH-PA Author Manuscript

NIH-PA Author Manuscript

promising method that has the potential to provide valuable information in a noninvasive manner.

Methods

Animal Preparations

All animal experiments were performed with institutional approval and in accordance with the ARVO Statement for the Use of Animals in Ophthalmic and Vision Research. The cat model for MR studies has been detailed elsewhere.[28,29] Briefly, six female adolescent cats (0.5–1.1 kg, 6–10 weeks old) were treated with atropine sulfate (0.05 mg/kg, intramuscularly) and anesthetized intramuscularly with a ketamine (10–25 mg/kg) and xylazine (2.5 mg/kg) cocktail. The forepaw vein was catheterized for fluid supplement. The animal was intubated and mechanically ventilated using a Harvard ventilator (35–45 stroke/min, 15–30 mL/stroke) under isoflurane anesthesia (~1.5% vol/vol) in a 50:50 N_2O-O_2 mixture, throughout the experiment. The isoflurane level used in this study was approximately 30% higher than that typically used in our fMRI studies of the cat visual cortex,[28,29] to reduce saccade-related motion artifacts. End-tidal P CO_2 was continuously monitored using a capnometer (Datex-Ohmeda, Louisville, CO) and kept within a normal physiological range (3%–4%). Atropine sulfate (1%), phenylephrine (2.5%), and proparacaine (0.5%, a topical anesthetic) eye drops were applied. The animal's eyes were refracted with corrective contact lenses (Danker Laboratory, Sarasota, FL). Polyethylene (PE)-10 tubing, filled with an atropine and proparacaine mixture (1:1), was secured at the corner of the eye for remote administration every 1 to 3 hours. The animal was then placed in a cradle and restrained in a normal postural position, using a head holder consisting of ear and mouth bars. The animal's rectal temperature was maintained at 38°C throughout the experiments. A typical fMRI study, including animal preparation, took 4 to 8 hours.

Stimulation Paradigm

The visual stimuli consisted of either stationary or drifting square-wave gratings (0.15 cyc/deg, 2 cyc/sec) of different orientations.[28–30] The stimulus contrast was approximately 100%. The control basal condition was a dark screen. The visual stimuli were projected onto a screen from the back of the magnet by a video projector (Resonance Technology Co., Northridge, CA). The screen was positioned at approximately 15 cm from the animal's eyes, covering approximately 37° of the visual field. Visual stimulation and image acquisition were synchronized using a homebuilt transistor–transistor logic input-output (TTL-I/O) device. In most studies the drifting-grating stimulus was used, with dark as the basal condition. In some experiments, a sequence of dark, drifting-, and stationary gratings were presented. Visual stimuli were presented to the full visual field, as well as to the upper and lower visual fields.

MR Experiments

fMRI experiments were performed on a 9.4-Tesla, 31-cm horizontal MRI scanner (Magnex Scientific, Abingdon, UK), equipped with a 30-Gauss/cm gradient (11.0 cm inner diameter, 300-μs rise time; Magnex Scientific), and a workstation console (^{Unity}INOVA; Varian, Palo Alto CA). A custom-built, small-surface coil was placed lateral to the right eye. Anatomic images were acquired using a data acquisition scheme (Turbo-FLASH) with an inversion–recovery contrast to suppress the strong signals from the vitreous humor for clear identification of the retinal–vitreous border. Sagittal anatomic images were acquired using the following parameters: interimage delay (TR), 3.5 seconds; flip angle, 10°; echo time (TE), 3.5 ms; inversion delay (TI), 1.4 seconds; data matrix, 128 × 128; and field of view (FOV), 3 × 3 cm^2. Typically, 9 to 12 sequential 1-mm anatomic images were acquired.

NIH-PA Author Manuscript

NIH-PA Author Manuscript

NIH-PA Author Manuscript

BOLD fMRI sagittal images were acquired using a gradient-echo, echo-planar imaging (EPI) data acquisition scheme,[31] with fat suppression and inversion-recovery contrast. EPI is widely used in fMRI studies, because it is more sensitive to stimulus-evoked T_2* and T_2 changes, and is less sensitive to physiological motion than other pulse sequences.[32] The single-shot, EPI sequence parameters were: TR, 3.5 seconds; TI, 1.4 seconds; TE, 12 ms; slice thickness, 1 or 2 mm; data matrix, 64 × 64; and FOV, 3 × 3 cm^2 (nominal in-plane resolution of 468 × 468 μm^2). Shifted-echo acquisition with the center echo at the 20th k-space line was used to achieve an echo time of 12 ms, approximating [33] Fat suppression was achieved tissue T_2* for optimal BOLD contrast. using three chemical-shift–selective (CHESS, 10-ms sinc) pulses and crusher gradients.[34] The strong signals from the vitreous humor were suppressed using a nonspatially selective inversion (10-ms hyperbolic secant) pulse with an inversion delay of 1.4 seconds. Typically, 3 to 12 multislice fMRI images were acquired in an interleaved fashion after a single-inversion pulse (total time for one multislice set was 3.5 seconds). Although there is a spread of TI values (1.4–1.7 seconds) across different slices, the vitreous signal was reasonably suppressed across multiple slices, because of its long T_1 at high field.

For the drifting gratings versus dark stimulus, a single fMRI measurement consisted of a three-epoch paradigm consisting of 20-20-20-20-20-20-20 images (underscore indicates drifting-grating stimulus is on). For the sequence of dark, drifting-, and stationary-grating stimuli, a single fMRI measurement consisted of two repeats of the following scheme: 20 images during dark, 20 images during drifting-grating, and 20 images during stationary-grating stimuli. Typically, approximately 15 repeated fMRI measurements were made on each animal.

Given these spatial resolutions, the term “retina” is used herein to refer to the retina–choroid complex. Although the inversion contrast used for suppression of the vitreous humor could yield a small contribution of blood flow to the fMRI signal, we refer to the fMRI signal as the BOLD signal, because our preliminary data suggested that the BOLD contribution was likely to be dominant (see the Discussion section).

Data Analysis

The EPI images were zero padded from a data matrix of 64 × 64 to 128 × 128. For data analysis programs written in commercial software were used (PV-Wave; Visual Numerics Inc., Boulder, CO) and Stimulate software.[35] Activation maps were computed by cross-correlation (CC) analysis in which pixel-by-pixel CC coefficients were calculated by matching the fMRI signal time course to the stimulus paradigm.[36] A CC threshold of 0.2, corresponding to P = 0.018, was used. A minimal cluster size for an active region of 8 pixels was further imposed, [37] yielding an effective P= 0.0017. All CC activation maps were overlaid on anatomic images. All time courses were generated from active pixels from the retina–choroid complex.

Multislice fMRI maps were reconstructed and flattened onto a two-dimensional plane. Regions of interests (ROIs) outlining the retina on the multislice anatomic images were manually drawn to guide the construction of a spherical surface representing the retina. For displaying the flattened retina, CC coefficients of each multislice activation map were rescaled from 0 to 1 to eliminate the gradual drop off in CC coefficients from lateral to medial, because of the surface–coil sensitivity profile. The rescaled activation map was projected onto the spherical surface and flattened by using a cartographic technique known as sinusoidal equal area projection.[38] The areas on the flattened map are conserved—that is, the areas of any subregions on the flattened maps are proportional to the corresponding areas on the spherical surface.

Results

Representative anatomic and the corresponding EPI images of the retina-choroid (sagittal view) are shown in Figures 1a and 1b, respectively. The inversion contrast incorporated in our

NIH-PA Author Manuscript

NIH-PA Author Manuscript

NIH-PA Author Manuscript

sequence suppressed the otherwise overwhelming strong signal from the vitreous body, allowing clear visualization of many detailed structures, such as the cornea, lens, vitreous body, and retina. Good-quality EPI images were obtained, with minimal geometric distortion or artifacts. Our first fMRI attempt of the retina in vivo, using drifting-grating stimulus without proparacaine and pancuronium, is shown in Figures 1c and 1d. Stimulus-evoked responses outlining the retina were detected with a single fMRI measurement. However, signal averaging of a few repeated measures was needed to generate robust activation maps. Typical percentages of change of the fMRI signals from the retina–choroid complex was 1.7% ± 0.1% ($P < 10^{-4}$, $n = 6$ cats). In addition to activation in the retina, nonspecific signal changes outside the retina were evident in the functional maps. These signal changes were probably associated with lens movement and saccadic motion, which occur even in animals under anesthesia.

In subsequent experiments, intravenous pancuronium and a topical proparacaine-atropine mixture were administered every 1 to 3 hours (in addition to isoflurane) to further minimize motion artifacts. Nine to 12 multislice fMRI studies were performed on three cats. Figure 2 (top) shows the functional maps from 8 of 12 consecutive, 1-mm slices of the retina after full-field stimulation of the drifting-grating stimulus in one representative animal. Note that the signal from the vitreous humor across multiple slices was reasonably suppressed with a single inversion. The visual stimuli activated a large area on the retina. The motion artifacts were markedly reduced with the addition of systemic paralytics and topical anesthetics. The multislice activation maps were reconstructed and flattened onto a two-dimensional surface (Fig. 2, bottom left). The flattened activation map was relatively uniform, and activity was not focally localized to the area centralis (analogous to the human fovea), probably because the stimulus was passively presented, and the anesthetized cat could not actively focus on the stimulus. Based on the anatomic images, the optic nerve head in the retina could be identified (data not shown). The optic nerve head was estimated to be approximately 2 mm in diameter. No statistically significant activation was observed in the anatomically identified optic nerve head (Fig. 2, bottom right, arrow). Note that there were a few single-pixel dark spots on the flattened activation map. However, they were scattered and significantly smaller than the optic nerve head, probably caused by noise fluctuation.

To further demonstrate that the fMRI maps of the retina were not artifacts, the upper and lower visual fields of the retina were separately stimulated with the drifting-grating stimulus ($n = 2$ cats). Figure 3 shows the results of the hemifield experiments. As expected, a stimulus presented in the upper half of the visual field predominantly stimulated the lower part of the retina, and stimulus presented in the lower half of the visual field predominantly stimulated the upper part of the retina. The separation between the upper and lower visual fields on the retina was distinct, but there was some overlap in the central visual field of the retina. Such an overlap could be a result of imperfect focus or fixation, saccadic motion artifact, and/or poor localization of the BOLD fMRI signals, to some extent. These questions remain to be investigated.

fMRI signal modulations due to drifting and stationary gratings were compared with the dark condition as a control. Figure 4 shows a time course after drifting- and stationary-grating stimuli compared with the dark condition. Positive signal changes were observed under both stationary and drifting gratings compared with the dark. The stimulus-evoked fMRI signal increase associated with the constant illumination, however, was significantly weaker (1.0% ± 0.1% versus 2.0% ± 0.3%, $P < 10^{-4}$, $n = 2$ cats, four epochs) than that associated with the drifting gratings. Correlation analysis of the functional maps showed only a few scattered pixels with negative signal changes along the retina. No consistent negative fMRI signal changes were observed in the retina (data not shown).

NIH-PA Author Manuscript

NIH-PA Author Manuscript

NIH-PA Author Manuscript

Discussion

fMRI of the retina is challenging. Major technical difficulties encountered in fMRI studies of the retina include imaging a thin curve tissue, imaging in regions of high-susceptibility distortion, signal contamination from fat and vitreous humor, and saccade-related motion artifacts. The retina is only approximately 250 μm thick; thus, high-resolution imaging must be used, resulting in relatively low signal-to-noise ratio. The use of a high field is helpful, because high fields increase the signal-to-noise and contrast-to-noise ratios. With a spatial resolution of 468 × 468 × 1000 μm^3, there are partial-volume effects that reduce functional contrast. Nevertheless, these data indicate that the fMRI signal is sufficiently strong to be readily detectable. The retina is physically located close to the nasal cavity and the frontal sinus, which are regions with large susceptibility differences, increasing the likelihood of image distortion. It is therefore critical to optimize the magnetic field homogeneity. A spin-echo acquisition scheme (instead of the gradient-echo scheme used herein) can be used to reduce signal loss due to intravoxel dephasing, although it is, in general, expected to yield a relatively poorer functional contrast. Major fat signals outlining the back of the eye can be reasonably suppressed using CHESS pulses and crusher gradients. Fat suppression eliminates chemical-shift ghost artifacts due to the resonance offset between the water and the fat signals. The strong signals from the vitreous humor can be efficiently suppressed with an inversion contrast, allowing a clear visualization of the retinal border and minimizing the partial volume effect by the otherwise overwhelming signal from the vitreous humor.

With regard to motion artifacts, saccadic motion is of primary concern. With an EPI acquisition scheme, which acquires the entire k-space data of one image within approximately 20 ms, motion within a single image is expected to be minimal. Saccadic and other potential motion artifacts between images can be significant, even under anesthetics, and can falsely correlate with the stimulus paradigm, as demonstrated in Figure 1. This observation is consistent with previous findings that systemic anesthetics are not completely effective in paralyzing the rectus muscles responsible for saccadic motion. However, with the addition of systemic paralytics and topical eye drop anesthetics, saccadic and lens motion were substantially and sufficiently reduced.

Although the BOLD response is likely to be dominant, there could be a small contribution from changes in blood-flow signal. Blood-flow weighting could arise from the use of a small surface coil for magnetization inversion, which could yield partial spatial selectivity, even for a nonspatially selective pulse. Such a blood flow–weighted signal would add constructively to the positive BOLD signal (if blood flow increased, as in activation of neurons in the cerebral cortex), resulting in increased functional contrast. Our preliminary data, however, suggest that blood flow's contribution under these experimental MR parameters is small (data not shown). Although this blood flow weighting does not compromise the potential of this method to image retinal function, separate measurements of BOLD and blood flow fMRI signals nevertheless should yield valuable information regarding the unique retinal metabolism and hemodynamics under basal and elevated activity conditions.

In an attempt to further understand the fMRI signal response under drifting and stationary stimuli, we measured the fMRI signal responses under drifting and stationary gratings compared with the dark. Both drifting and stationary gratings evoked an increase in the BOLD (oxygenation) response compared with the dark condition. Our observation is consistent with that of Bill and Sperber[39] who used deoxyglucose technique and found that flickering light evokes a higher metabolic rate in the inner retina than steady light. Our observation is also in accordance with that of Stefansson,[40] who used an oxygen electrode to measure preretinal oxygenation changes as a function of the room light intensity and found that oxygen tension increases with increasing room light intensity compared with darkness. It should be noted that

NIH-PA Author Manuscript

NIH-PA Author Manuscript

NIH-PA Author Manuscript

a simple illumination compared with dark is generally known to result in hyperpolarization of the photoreceptors and, thus, a decrease in metabolism. Consequently, a decrease in fMRI signal is expected compared with dark. Our data showed, on the contrary, that the fMRI signal change is positive under constant illumination compared with dark, suggesting there is an overall regional metabolic and blood flow increase. One possible explanation for this discrepancy is that hyperpolarization, per se, evokes a net metabolic increase (and commensurately larger blood flow increase) in the photoreceptors and/or in other cell types (such as bipolar and horizontal cells) along signal transduction pathway. Another possibility is that the electrophysiogical and fMRI measurements might not be measuring the same parameters, in that hyperpolarization is recorded from the photoreceptors, whereas the fMRI signal samples the entire retinal tissue. The difference in stimuli used in the electrode recording and our fMRI measurements could be a factor. Further studies are needed to fully understand the fMRI signal changes. Comparison across different modalities under identical or similar experimental conditions is necessary to determine whether there are indeed discrepancies between these measurements.

The retina is nourished by the retinal and choroidal blood supplies.[4] The choroidal blood flow, which nourishes the photoreceptors, is many times higher than the retinal blood flow[8–10] (4–10 times, depending on species and regions on the retina). The fMRI signal changes could originate from the choroidal and/or the retinal vessels. At current spatial resolution, it is not yet possible to separate the choroidal and retinal contributions to the fMRI signal. We are working on increasing spatial resolution in an attempt to resolve these contributions. Understanding the sources and mechanisms underpinning the fMRI signal changes in the retina is important for designing better experiments and for making full use of this method for imaging retinal “function.”

Conclusions

We developed a noninvasive fMRI method for dynamically imaging retinal function and physiology serially in three dimensions. Although much work remains to further understand the fMRI signal sources, the methodology demonstrated herein has the potential to provide a novel and noninvasive mean to investigate retinal function and physiology under normal and disease states, such as diabetic retinopathy, glaucoma, and macular degeneration. With improved spatial resolution, it could also be used to visualize noninvasively the detailed functional organization of the retina, such as layer-specific activity and horizontal interactions. This methodology also has the potential to complement current existing modalities.

Acknowledgments

Supported by National Institutes of Health Division of Research Resources Grant RR08079, National Institute of Neurological Disorders and Stroke Grants NS38295 and NS10930, and the Keck Foundation.

References

1. Wassle H, Boycott BB. Functional architecture of the mammalian retina. Physiol Rev 1991;1:447–480. [PubMed: 2006220]
2. Foulds WS. The choroidal circulation and retinal metabolism: an overview. Eye 1990;4:243–248. [PubMed: 2199233]
3. Wise, GN.; Dollery, CT.; Henkind, P. The Retinal Circulation. New York: Harper and Row; 1971. Structure of retinal vessels; p. 34-54.
4. Harris A, Kagemann L, Cioffi GA. Assessment of human ocular hemodynamics. Surv Ophthalmol 1998;42:509–533. [PubMed: 9635901]
5. Linsenmeier RA. Effects of light and darkness on oxygen distribution and consumption in the cat retina. J Gen Physiol 1986;88:521–542. [PubMed: 3783124]

NIH-PA Author Manuscript

NIH-PA Author Manuscript

NIH-PA Author Manuscript

6. Stefansson E. Oxygen and diabetic eye disease. Graefes Arch Clin Exp Ophthalmol 1990;228:120–123. [PubMed: 2186971]
7. Schmettterer L, Wolzt M. Ocular blood flow and associated functional deviations in diabetic retinopathy. Diabetologia 1999;42:387–405. [PubMed: 10230642]
8. Alm A, Bill A. Blood flow and oxygen extraction in the cat uvea at normal and high intraocular pressures. Acta Physiol Scand 1970;80:19–28. [PubMed: 5475327]
9. Friedman E, Kopald HH, Smith TR. Retinal and choroidal blood flow determined with krypton 85 in anesthetized animals. Invest Ophthalmol 1964;3:539–547. [PubMed: 14229941]
10. Roth S, Pietrzyk Z. Blood flow after retinal ischemia in cats. Invest Ophthalmol Vis Sci 1994;36:1904–1909.
11. Alm A, Bill A. The oxygen supply to the retina. II: effects of high intraocular pressure and of increased arterial carbon dioxide tension on uveal and retinal blood flow in cats. Acta Physiol Scand 1972;84:306–319. [PubMed: 4553229]
12. Parver LM. Choroidal blood flow as a heat dissipating mechanism in the macula. Am J Ophthalmol 1980;89:641–646. [PubMed: 6769334]
13. Parver LM, Auker CR, Carpenter DO, et al. Choroidal blood flow. Arch Ophthalmol 1982;100:1327–1330. [PubMed: 7103819]
14. Birch, DG. Focal electroretinography. In: Heckenlively, JR.; Arden, GB., editors. Principles and Practice of Clinical Electrophysiology of Vision. St. Louis: Mosby; 1991. p. 334-338.
15. Bearse MAJ, Sutter EE. Imaging localized retinal dysfunction with the multifocal electroretinogram. J Opt Soc Am A 1996;13:634–640.
16. Vo VT, Riva CE. Variations of blood flow at optic nerve head induced by sinusoidal flicker stimulation in cats. J Physiol 1994;482:189–202.
17. Riva CE, Harino S, Petrig BL, et al. Laser Doppler flowmetry in the optic nerve. Exp Eye Res 1992;55:499–506. [PubMed: 1426079]
18. Riva CE, Petrig BL. Blue field entoptic phenomenon and blood velocity in the retinal capillaries. J Opt Soc Am A 1990;70:1234–1238.
19. Preussner PR, Richard G, Darrelmann O, et al. Quantitative measurement of retinal blood flow in human beings by application of digital image-processing methods to television fluorescein angiograms. Graefes Arch Clin Exp Ophthalmol 1983;221:110–112. [PubMed: 6689414]
20. Berkowitz BA, Wilson CA. Quantitative mapping of ocular oxygenation using magnetic resonance imaging. Magn Reson Med 1995;33:579–581. [PubMed: 7776892]
21. Ogawa S, Lee T-M, Kay AR, et al. Brain magnetic resonance imaging with contrast dependent on blood oxygenation. Proc Natl Acad Sci USA 1990;87:9868–9872. [PubMed: 2124706]
22. Ogawa S, Tank DW, Menon R, et al. Intrinsic signal changes accompanying sensory stimulation: functional brain mapping with magnetic resonance imaging. Proc Natl Acad Sci USA 1992;89:5951–5955. [PubMed: 1631079]
23. Kwong KK, Belliveau JW, Chesler DA, et al. Dynamic magnetic resonance imaging of human brain activity during primary sensory stimulation. Proc Natl Acad Sci USA 1992;89:5675–5679. [PubMed: 1608978]
24. Bandettini PA, Wong EC, Hinks RS, et al. Time course EPI of human brain function during task activation. Magn Reson Med 1992;25:390–397. [PubMed: 1614324]
25. Riva CE, Harino S, Shonat RD, et al. Flicker evoked increase in optic nerve head blood flow in anesthetized cats. Neurosci Let 1991;128:291–196. [PubMed: 1945050]
26. Longo A, Geiser M, Riva CE. Subfoveal choroidal blood flow in response to light-dark exposure. Invest Ophthalmol Vis Sci 2000;41:2678–2683. [PubMed: 10937582]
27. Scheiner AJ, Riva CE, Kazahaya K, et al. Effect of flicker on macular blood flow assessed by the blue field simulation technique. Invest Ophthalmol Vis Sci 1994;35:3436–3441. [PubMed: 8056519]
28. Duong TQ, Kim D-S, Ugurbil K, et al. Spatio-temporal dynamics of the BOLD fMRI signals in cat visual cortex: toward mapping columnar structures using the early negative response. Magn Reson Med 2000;44:231–242. [PubMed: 10918322]
29. Kim D-S, Duong TQ, Kim S-G. High-resolution mapping of iso-orientation columns by fMRI. Nat Neurosci 2000;3:164–169. [PubMed: 10649572]

NIH-PA Author Manuscript

NIH-PA Author Manuscript

NIH-PA Author Manuscript

30. Malonek D, Grinvald A. Interactions between electrical activity and cortical microcirculation revealed by imaging spectroscopy: implication for functional brain mapping. Science 1996;272:551–554. [PubMed: 8614805]

31. Mansfield P. Multi-planar image formation using NMR spin echoes. J Phys C: Solid State Phys 1977;10:L55–L58.

32. Callaghan, PT. Principles of Nuclear Magnetic Resonance Microscopy. Vol. chap 3. Oxford, UK: Clarendon Press; 1991.

33. Menon RS, Ogawa S, Tank DW, et al. 4 Tesla gradient recalled echo characteristics of photic stimulation-induced signal changes in the human primary visual cortex. Magn Reson Med 1993;30:380–386. [PubMed: 8412612]

34. Moonen C, van Zijl P. Highly effective water suppression for in vivo proton NMR spectroscopy (DRYSTEAM). J Magn Reson 1990;88:28–41.

35. Strupp JP. Stimulate: a GUI based fMRI analysis software package (Abstract). Neuroimage 1996;3:S607.

36. Bandettini PA, Jesmanowicz A, Wong EC, et al. Processing strategies for time-course data sets in functional MRI of human brain. Magn Reson Med 1993;30:161–173. [PubMed: 8366797]

37. Forman SD, Cohen JD, Fitzgerald M, et al. Improved assessment of significant activation in functional magnetic resonance imaging (fMRI): use of a cluster-size threshold. Magn Reson Med 1995;33:636–647. [PubMed: 7596267]

38. Bugayevskiy, LM.; Synder, JP. Map Projections: A Reference Manual. London: Taylor and Francis; 1995.

39. Bill A, Sperber GO. Aspects of oxygen and glucose consumption in the retina: effects of high intraocular pressure and light. Exp Ophthalmol 1990;228:124–127.

40. Stefansson E. Retinal oxygen tension is higher in light than in dark. Pediatr Res 1988;23:5–8. [PubMed: 3340444]

NIH-PA Author Manuscript
NIH-PA Author Manuscript
NIH-PA Author Manuscript

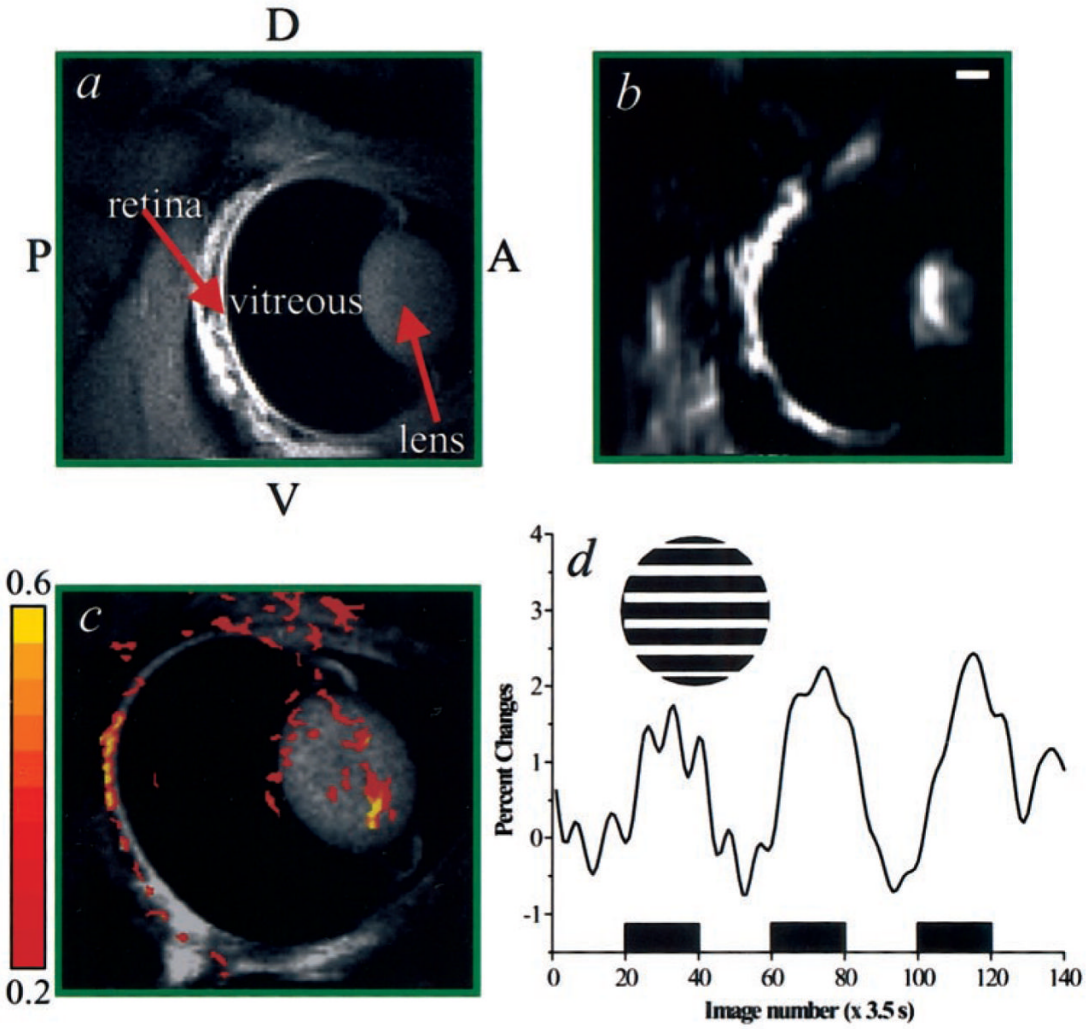

Figure 1.

Anatomic (**a**) and corresponding echo-planar (**b**) images, at 234 × 234 × 1000 μm^3 and 468 × 468 × 1000 μm^3, respectively. The cornea, lens, vitreous humor, and retina are clearly depicted in the anatomic image. (**c**) First attempt to obtain an fMRI of the retina under drifting versus dark stimulation without systemic paralytics and topical anesthetics. The cross-correlation activation map (468 × 468 × 2000 μm^3) of the retina is overlaid on an anatomic image. The color pixels reflect cross-correlation coefficients, as indicated by the color bar. Functional responses from the retina are clearly depicted, with increased activity along the retinal tissue. Artifacts associated with lens movement and saccadic motion outside the retina are also evident. (**d**) fMRI time course associated with a three-epoch stimulation (indicated by the *black boxes*) paradigm obtained from active pixels in the retina. The percentage change ranges from 1.5% to 2.0%. *Inset*: grating stimulus of one orientation (0°). The stimulus was actually drifting. P, posterior; A, anterior; D, dorsal; V, ventral. Scale bar, 2 mm.

NIH-PA Author Manuscript

NIH-PA Author Manuscript

NIH-PA Author Manuscript

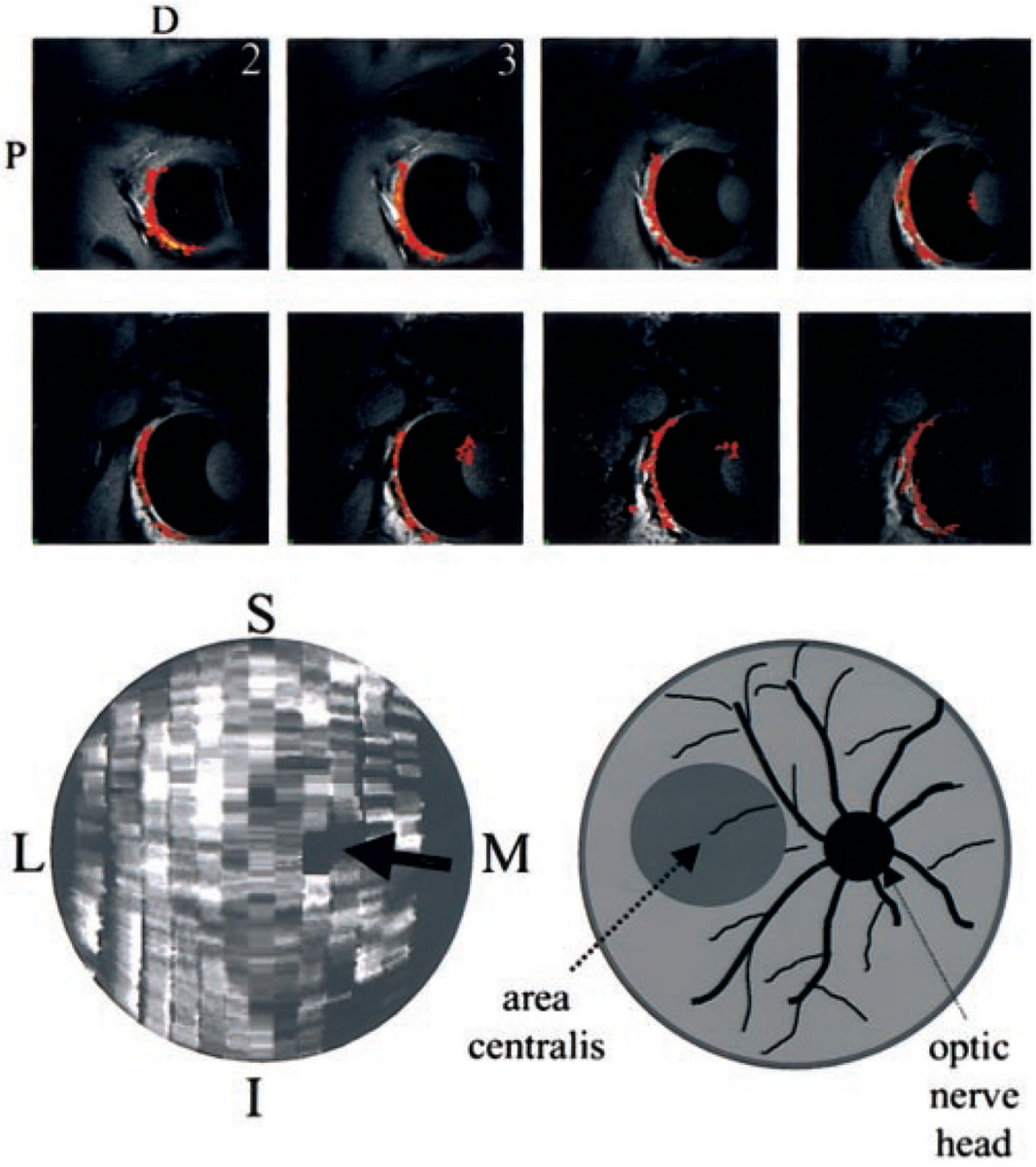

Figure 2.

Top: Multislice fMRI maps of the retina with systemic paralytics and topical anesthetics. Functional maps from 8 of 12 consecutive, 1-mm slices of the retina were obtained associated with full-field stimulation of drifting gratings (versus dark). Cross-correlation activation maps ($468 \times 468 \times 1000\ \mu m^3$) of the retina are overlaid on anatomic images. The drop off in signal-to-noise ratio, and thus statistical certainty, from slice 1 to slice 8 (lateral to medial) is associated with the asymmetric sensitivity profile of the surface coil. *Bottom*: Reconstructed and flattened activation map of the retina (*left*). Relatively uniform activation was observed across the retina. The optic nerve head (*black arrow*) was identified based on anatomy. No statistically significant activation was observed in and around the anatomically identified optic nerve head. M, medial; L, lateral; S, superior; I, inferior. The schematic representation (*right*) is for the reader's convenience.

NIH-PA Author Manuscript

NIH-PA Author Manuscript

NIH-PA Author Manuscript

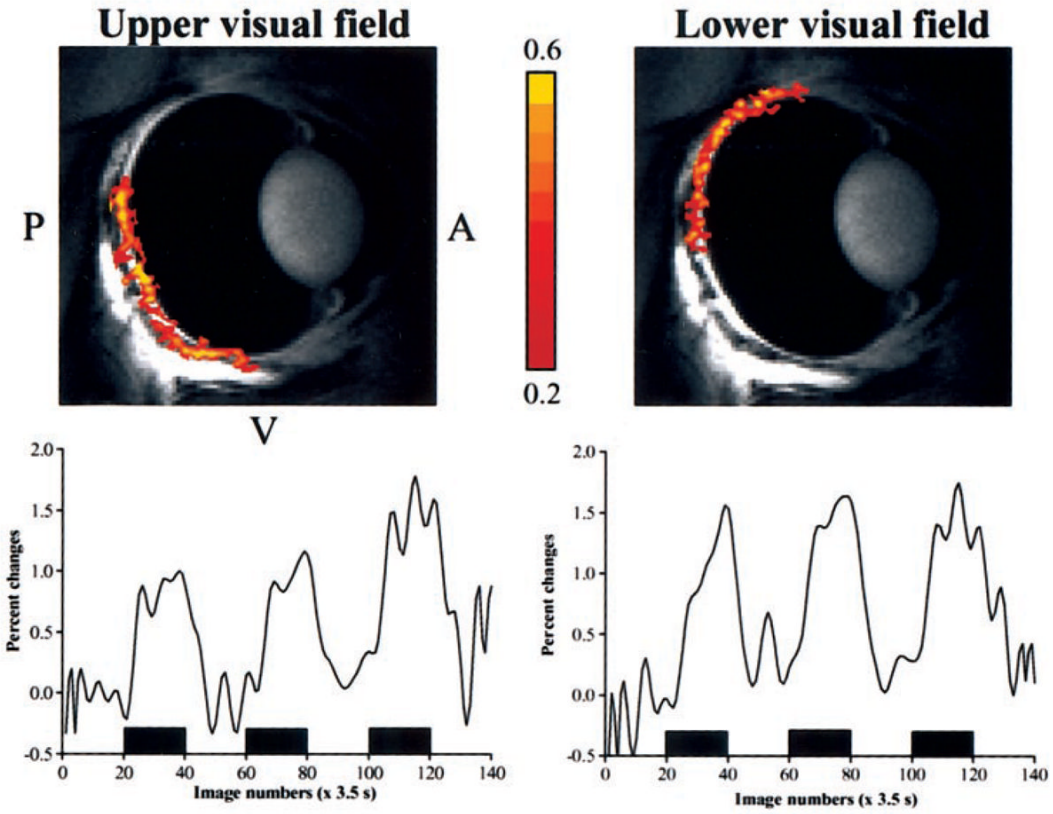

Figure 3.

fMRI maps (468 × 468 × 1000 μm^3) of the upper and lower visual fields using drifting versus dark stimulation (*top*), with percentage changes in signals between the two conditions (*bottom*). The stimulus presented to the upper visual field activated the bottom half of the retina, and that presented to the lower visual field activated the upper part of the retina. The color pixels reflect cross-correlation coefficients as indicated by the color bar. P, posterior; A, anterior; V, ventral.

NIH-PA Author Manuscript

NIH-PA Author Manuscript

NIH-PA Author Manuscript

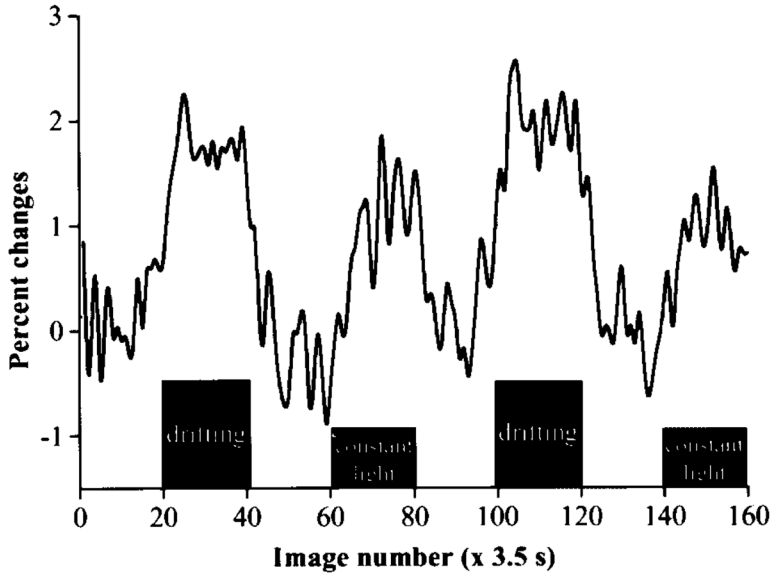

Figure 4.

fMRI signal modulation under dark, drifting grating, and constant illumination. Positive signal changes were observed under both drifting grating and constant illumination stimuli compared with dark basal conditions. Signal change associated with the drifting grating (~2%) was approximately twice that associated with the stationary grating (~1.1%).